Journal of Materials Chemistry A

PAPER

View Article Online
View Journal | View Issue

Cite this: J. Mater. Chem. A, 2017, 5, 14611

A scheme for the generation of Fe–P networks to search for low-energy $LiFePO_4$ crystal structures

Xiaobao Lv,[ab] Xin Zhao,[b] Shunqing Wu,[c] Ping Wu,[d] Yang Sun,[b] Manh Cuong Nguyen,[b] Yongliang Shi,[ae] Zijing Lin,*[a] Cai-Zhuang Wang[b] and Kai-Ming Ho*[de]

Received 22nd March 2017
Accepted 28th May 2017

DOI: 10.1039/c7ta02532g

rsc.li/materials-a

Herein we present a network generation scheme to explore the structural diversity of $LiFePO_4$, which is an important cathode material in Li-ion batteries. With our scheme, networks of Fe and P atoms were initially constructed as the backbone structures using structural motifs for the FeP_x and FeP_x configurations, obtained from existing structural databases. Then, O atoms were added, resulting in the formation of PO_4 tetrahedra and different types of Fe–O polyhedra. Finally, Li atoms were inserted into the vacancies within the generated $FePO_4$ structures. We searched structures with FeO_4, FeO_5, or FeO_6 polyhedra (unit cell with sizes of up to 4 formula units) and obtained ~8 times more low-energy structures through our database than through existing databases. Furthermore, using our more comprehensive structural database, we unveiled a number of rules for identifying low-energy structures. These improved results complement the existing databases and are valuable for further research on structural transformations in similar materials by changing lithium or sodium cation populations.

1. Introduction

Materials informatics is a new initiative, which has recently attracted a lot of attention in scientific research. The basic strategy is to construct comprehensive data sets and use machine learning to solve a wide variety of problems in materials design and discovery. To achieve this, a key element is the quality and comprehensiveness of the databases. One of the most advanced databases is that of materials used in lithium-ion batteries, in particular, lithium iron phosphate ($LiFePO_4$), which has been one of the main cathode materials for commercial Li-ion batteries since their introduction in 1997.[1] In this study, we examined the Materials Project (MP) database,[2] which is currently regarded as the most comprehensive database on the structures of materials for batteries. It contains 60 experimental or hypothetical $LiFePO_4$ crystal structures within an energy window of 0.7 eV/f.u. (formula unit) above the ground-state olivine structure.

Compared with $LiCoO_2$-based materials, $LiFePO_4$ presents the advantage of being safer, and having a longer cycle life and lower costs.[3–7] The ground state phase of $LiFePO_4$ is known as the olivine structure (α-phase),[1] shown in Fig. 1(a). In addition, a high-pressure and high-temperature phase, known as β-phase (Fig. 1(b)), has also been reported.[8] Although $LiFePO_4$ is expected to exhibit a rich polymorphism, similarly to the silicate system (*e.g.* Li_2FeSiO_4),[9] no stable structures other than α- and β-$LiFePO_4$ have been found experimentally. A comprehensive crystal structure database is the key to understand the structural diversity of this system and assist the analysis of structural transformations during charge/discharge cycling. Due to the importance of $LiFePO_4$, several hypothetical crystal structures have been proposed, and all of them have been added to the MP database. However, less than half of these configurations are within an energy window of 0.35 eV/f.u., which corresponds to approximately 600 K in terms of temperature and therefore, is

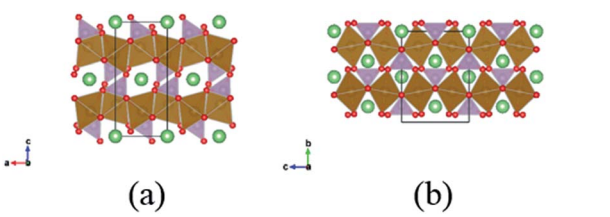

Fig. 1 Experimental phases of $LiFePO_4$: (a) α-phase (the ground state), also known as the olivine phase; (b) β-phase. Atom color code: Fe atoms and FeO_x polyhedral, brown; P atoms and PO_4 tetrahedra, purple; Li atoms, light green; O atoms, red.

[a]CAS Key Laboratory of Strongly-Coupled Quantum Matter Physics, Department of Physics, University of Science and Technology of China, Hefei 230026, China. E-mail: zjlin@ustc.edu.cn

[b]Ames Laboratory, US DOE, Ames, Iowa 50011, USA

[c]Collaborative Innovation Center for Optoelectronic Semiconductors and Efficient Devices, Department of Physics, Xiamen University, Xiamen 361005, China

[d]International Center for Quantum Design of Functional Materials (ICQD), Hefei National Laboratory for Physical Sciences at the Microscale, University of Science and Technology of China, Hefei 230026, China. E-mail: kmh@iastate.edu

[e]Department of Physics and Astronomy, Iowa State University, Ames, Iowa 50011, USA

the most relevant energy window for battery applications. Among these low-energy structures, 19 of them have no more than 4 formula units (*i.e.*, 28 atoms) per unit cell. In this study, we managed to extend the existing database by exploring the structural diversity in the $LiFePO_4$ system using a novel network generation scheme.

Recently, Ye *et al.* examined the X-ray diffraction data of Na_2FeSiO_4 materials obtained during charge/discharge cycling[10] in batteries and found that although many different crystal structures exist in these materials, they all possess a common diamond-like Fe–Si network. Further study by Wu *et al.* showed that low-energy Na_2FeSiO_4 crystal structures can be classified into groups with similar electrochemical properties according to their Fe–Si networks.[11] This new perspective presented in the studies on silicates motivated our development of a structure search scheme for the phosphate system based on Fe–P networks. While previous studies showed that low-energy structures of Li_2FeSiO_4 can be easily generated from a tetrahedral network,[9] this is not applicable to the $LiFePO_4$ system, where a diverse local environment with the presence of multiple types of oxygen polyhedra around the cations (Li and Fe) leads to a much more complex structural landscape. In this context, herein we report a new scheme based on Fe–P networks that is applicable to the analysis of this extremely complex system. In a search for crystal unit cells with up to 28 atoms, our scheme located eight times more low-energy structures than existing databases (within 0.35 eV/f.u above the ground state olivine structure). Thus, the powerful search capability of this method facilitates the sampling of the low-energy/low-temperature structural landscape.

2. Methods

2.1 Fe–P networks in MP database

To extend the number of low-energy structures in the existing database, we first examined the nature of the Fe–P networks in the structures of the MP database. Some typical examples of Fe–P networks for $LiFePO_4$ are shown in Fig. 2. We found that $LiFePO_4$ has a very stable tetrahedral PO_4 motif, with no shared atoms between the different tetrahedra, such that the phosphate PO_4 ion can be considered as a single unit. Fe and O atoms form mainly FeO_6 and FeO_4 polyhedra. For the structures containing FeO_6, PO_4 and FeO_6 polyhedra share the corners or the edges (no face-sharing geometries were found in the MP database). If all neighboring O to FeO_6 share corners, this results in an octahedral Fe–P arrangement. On the other hand, if PO_4 and FeO_6 share one edge, this results in one less Fe–P linkage, giving a FeP_5-type structure. Moreover, neighboring O sharing two edges can produce either a planar or tetrahedral FeP_4 configuration, depending on which edges are shared in the FeO_6 octahedron. Finally, all FeO_4-type structures feature arrangements where PO_4 and FeO_4 share corners, resulting in a tetrahedral FeP_4 configuration. Some examples of these configurations are shown in Fig. 3. The Fe–P configurations also have some special shapes. Bond angle clustering analysis performed for these FeP_x and PFe_x configurations yielded a series of typical averaged configurations, with bond lengths and bond angles listed in Table 1 in the Appendix.

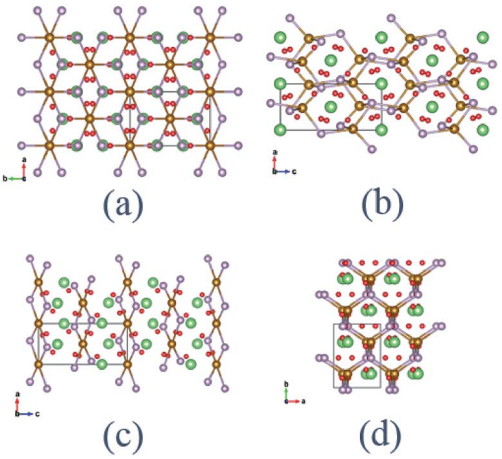

Fig. 2 Examples of Fe–P networks in some of the $LiFePO_4$ structures from the MP database: (a) FeP_6-type network; (b) FeP_5-type network; (c) FeP_4-type network; (d) another FeP_4-type network. Structures (a–c) all have FeO_6 polyhedra and (d) has FeO_4 polyhedra. Note that Fe and P do not form direct bonds within $LiFePO_4$, and are linked *via* the intermediate O atoms.

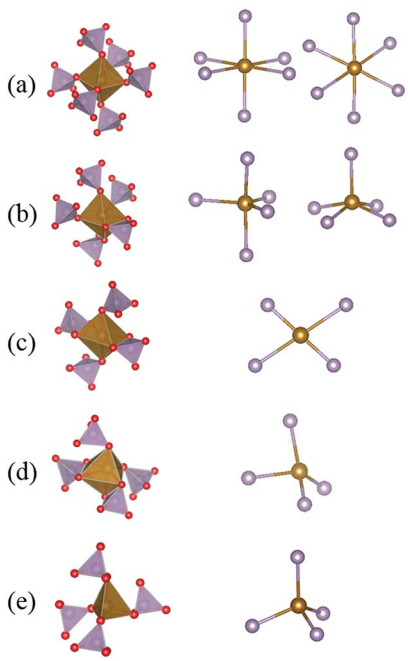

Fig. 3 Connections between P-centered and Fe-centered polyhedra, and the corresponding Fe–P configurations in known $LiFePO_4$ structures: (a) corner-sharing; (b) one edge-sharing; (c) two edge-sharing; (d) two edge-sharing (e); corner-sharing. In this diagram, the Fe atom and its neighboring PO_4 tetrahedra are isolated from the crystal. The left column shows the different FeO and PO polyhedra, and the right column shows the corresponding Fe–P configurations. Atom color code: Fe atoms and FeO_x polyhedral, brown; P atoms and PO_4 tetrahedra, purple; Li atoms, light green; O atoms, red.

2.2 Generation of the Fe–P network

To generate the desired Fe–P networks, we used an approach similar to that of the published code GRINSP,[12] which has been successfully applied in the study of zeolite-type structures. In our code, Fe–P networks were generated according to each crystal symmetry space group using the Monte Carlo method. First, the code builds an empty cell. The lattice parameters of the cell are restricted by its symmetry and within a range according to the number of atoms in the cell (details provided in the Appendix). Second, Fe and P atoms are successively added to the empty cell using symmetry operations. This step is repeated until the required coordination numbers (CN) for Fe and P are reached. If the CN exceeds the required number, the entire process starts over until a Fe–P network with an acceptable CN is formed. Subsequently, the network was examined to ensure that all FeP_x and PFe_x configurations were within the preset tolerance for the typical averaged configurations listed in Table 1 in the Appendix. Finally, duplicate networks were removed. The flowchart for the network-generation code is presented in Fig. 4. More details about network generation, elimination criteria and procedures are described in the Appendix. The qualifying networks were submitted to the next step.

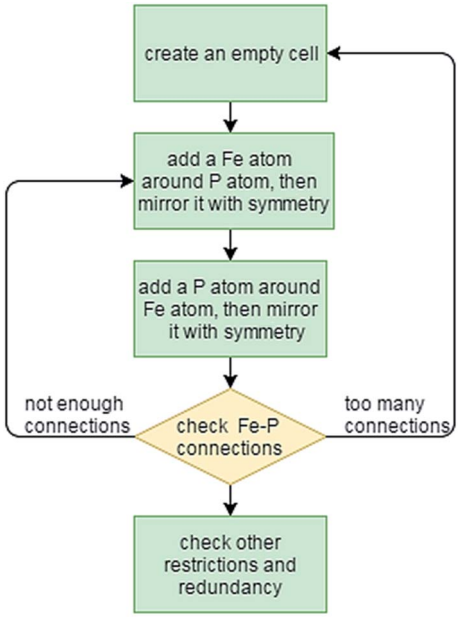

Fig. 4 Flowchart for the network-generated code. Fe and P atoms are randomly placed in an empty cell and the Fe–P coordination number should be equal to the required number (4, 5 or 6). Note that the newly generated configurations only contain Fe and P atoms at this step.

2.3 Adding oxygen atoms

After the Fe–P networks were generated, four O atoms were added around each P atom to create a rigid PO_4 tetrahedron. These PO_4 tetrahedra were rotated around the fixed P atoms to form FeO_x polyhedra with the neighbouring Fe atoms. To efficiently determine the best PO_4 orientation, a genetic algorithm[13] was applied. For simplicity, the crossover operation was only performed on the orientations of the PO_4 tetrahedra, as schematically depicted in Fig. 5. Meanwhile, a restricted force field relaxation by the LAMMPS[14] code was applied to the newly generated structures. During the relaxation, the Fe–P network was fixed while the PO_4 rigid tetrahedra rotated around the fixed P atoms. The force field used in this investigation was obtained from preliminary adaptive genetic algorithm (AGA)[15] studies for $LiFePO_4$. Details for the force field are included in the Appendix.

2.4 Adding lithium atoms

Finally, Li atoms were added to the $FePO_4$ structures obtained in the previous step. The potential vacancy sites within the $FePO_4$ structure were located by dividing the $FePO_4$ cell into a 3D mesh grid. Grid sites with a distance to other atoms larger than a certain value (see Appendix) were considered as vacancies, where Li atoms were randomly inserted.

The final $LiFePO_4$ structures obtained through the above scheme were fully relaxed by first principles calculations. In the final structure pool, the Li and Fe positions were switched in the low-energy structures so as to acquire more structures. More details can be found in the Appendix.

3. Results and discussion

3.1 Structure search results in our database *vs.* the MP database

The energies of the DFT-relaxed structures relative to the ground state olivine structure were plotted against their corresponding volumes, as shown in Fig. 6. Compared to the MP database (Fig. 6(b)), which only contains 19 structures (with 28 atoms or less in the unit cell) under 0.35 eV/f.u., a search in our database returned 158 structures, *i.e.*, 8 times more structures than in the MP database. As shown in Fig. 6(a), within the energy range of 0.20 eV/f.u., our search results contained all 10 structures from the MP database, including the experimental

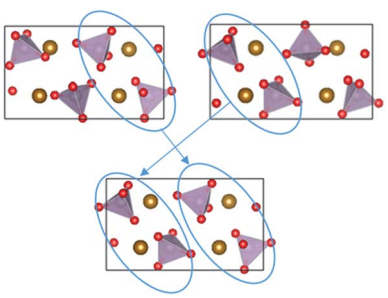

Fig. 5 Crossover operation of the genetic algorithm for determining the best orientation of the PO_4 tetrahedra. The top two are the parent arrangements and the bottom one is the child arrangement. Arrangements with lower classical potential energy were selected for a crossover. The only change in this operation was the orientation of the PO_4 tetrahedra, while the Fe–P network remained fixed.

α and β phases. In addition, 46 new structures were found in the energy window of 0.20 eV/f.u.

3.2 Bond length analysis

In the first step to classify the structures in this complex database, we performed an analysis of the cation-O and Fe–P bond lengths among 3 different groups of structures, classified according to their energy. The collective results are shown in Fig. 7. The differences in the P–O bond length were very small among the different groups, indicating that the tetrahedral PO_4 anion is a well-defined subunit. The peak at 1.552 Å for P–O is relatively sharp compared to that of other atom pairs. We set the cutoff length for the P–O bond at 1.8 Å. For Fe–O, the peak at 2.05 Å, corresponding to the first neighbor bond distances, has a small tail that extends to 2.7 Å. Therefore, 2.7 Å was selected as the cutoff bond length for the Fe–O polyhedra. Likewise, the Li–O cutoff bond length was set at 2.6 Å. For Fe–P, the spread in bond length reflects the variety of networks, but the bond length distribution is still largely consistent with the parameters listed in Table 1 (Appendix).

3.3 The low-energy structural landscape of $LiFePO_4$

Using the above bond cutoff distances, we replotted the results shown in Fig. 6(a) with the structures classified according to the type of Fe–O polyhedra (Fig. 8). It can be seen that the low energy structures under 0.2 eV/f.u. are located in two valleys, one at a volume of about 75 $Å^3$/f.u. (corresponding to FeO_6 structures), and the other at a larger volume of about 90 $Å^3$/f.u. (corresponding to FeO_4 structures). Both experimentally observed structures are at the smaller volume valley, corresponding to FeO_6. However, the energies of the two types of structures are actually very close, indicating that further research to investigate the possibility of synthesizing FeO_4-type structures may be worthwhile. Meanwhile, within the 0.2 eV/f.u. energy window, there are much fewer structures in the FeO_6 valley than in the FeO_4 valley. This can be traced to the different behavior of the two types of structures during the Li–Fe switching process, due to the Li and Fe environments being very different in the FeO_6-type structures. In most of these structures, Li atoms form LiO_4 tetrahedra while Fe forms FeO_6 octahedra. For the ground state structure, although both Fe and Li are bonded to 6 oxygens, the

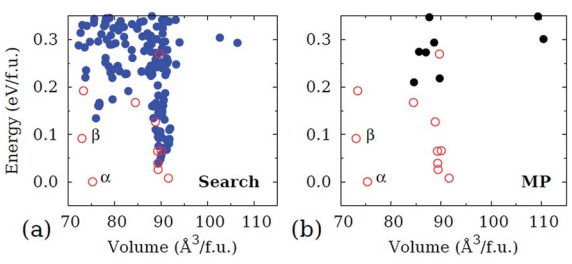

Fig. 6 Energy *vs.* volume plot of the structures in (a) our database and (b) the MP database. The unit cells of the structures contain up to 28 atoms. Red open circles denote structures found in both databases. Solid blue circles denote those structures found only in our database. The two experimental phases are the ones labeled as α and β.

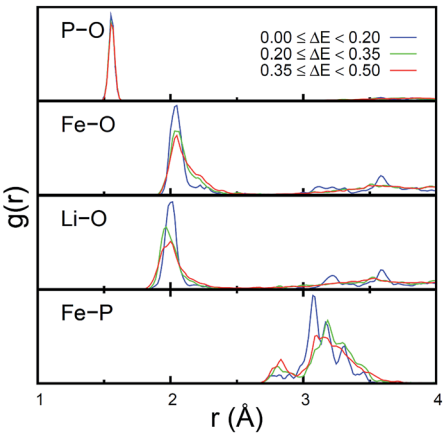

Fig. 7 Distribution function of the atom distances in the $LiFePO_4$ structures from our database with an energy of up to 0.50 eV/f.u. above ground state. The cations-O and Fe–P distances in the network were analyzed. The dataset was divided into 3 groups according to the relative energies above ground state (Δ*E*, eV/f.u.).

FeO_6 polyhedra share one edge and four corners with the surrounding PO_4 tetrahedra, while the LiO_6 polyhedra share two edges and two corners with the surrounding PO_4 tetrahedra, which results in different Fe–P distances. These differences in the Li and Fe environment lead to a substantial energy increase after switching Li and Fe. On the other hand, in the FeO_4-type structure, Li and Fe have a nearly equivalent local environment. Both Li and Fe have 4 oxygen atoms at a distance of about 2.0 Å, and all LiO_4 and FeO_4 tetrahedra share corners with the PO_4 tetrahedra. Therefore, FeO_4-type structures where Li and Fe have been switched still have relatively low energies, resulting in a much richer polymorphism at low energies compared to the FeO_6-type structures. As regards structural stability, such rich polymorphism within a narrow energy range may indicate that it is easier for a phase transition to occur during a Li charge/discharge

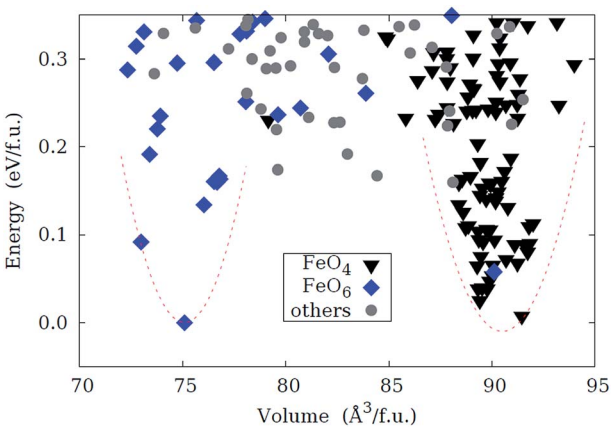

Fig. 8 $LiFePO_4$ structures under 0.35 eV/f.u. obtained from our database. The Fe–O coordination number can be either 4 (marked with black triangles), 6 (marked with blue squares) and a combination of 4, 5, and 6 (marked with gray dots). The volume range is set to 95 $Å^3$/f.u. Two red curves are plotted to show the distribution of the lowest-energy structures.

cycle, which can make FeO_4-type structures less stable during battery operation.

The two valleys are separated by a plateau of about 0.2 eV/f.u., where a mixture of FeO_4-type, FeO_5-type, and FeO_6-type structures coexist. These structures may be transition states, which possibly appear during the structural transition between FeO_6-type and FeO_4-type structures.

3.4 Dynamical stability

To examine the stability of the FeO_4 structures in the right valley, we selected the two structures in this valley with the lowest energy to calculate the phonon density of states, and the ground state olivine-type structure was selected for reference. Fig. 9 shows the phonon density of states of these structures, where it can be seen that all three structures were dynamically stable.

3.5 The energy rules

By extending the analysis to a larger energy window (0.7 eV/f.u.), with more than 900 structures, several rules for selecting low-energy $LiFePO_4$ structures based on local atom connections were identified. In Fig. 10, those structures violating the rules are represented in gray (labeled as 'others') and white (labeled as 'v-FeO_6' or 'v-FeO_4'). Firstly, we noticed that almost all low-energy structures (below 0.2 eV/f.u.) in Fig. 10(b) contained six- or four-coordinated Fe atoms to O atoms, whereas in the larger energy window (up to 0.7 eV/f.u.), the variety of motifs or mixture of motifs is much wider, as shown in Fig. 10(a). By applying this rule, a 51.7% of the structures (labeled as 'others' in Fig. 9(a)) were removed from our database of 900. The second rule consists in that Li atoms should also be bonded to either 6 or 4 oxygen atoms. The third rule specifies that each oxygen atom should be linked to 3 cations in the FeO_4-type structures and 3 to 4 cations in the FeO_6 type structures. By applying the second and third rules, 8.3% of the FeO_6-type structures (labeled as 'v-FeO_6') and 20.8% of the FeO_4-type structures (labeled as 'v-FeO_4') were screened out, as shown in the pie chart of Fig. 10(a). By applying the above three rules, about 80% of the 900+ examined structures were screened out with only a small loss (4 structures labeled as 'others' in Fig. 10(b)) in the low-energy window (<0.2 eV/f.u.). These rules lead to a more uniform cation distribution in geometry[2] and can dramatically improve the efficiency of structure generation in our search scheme.

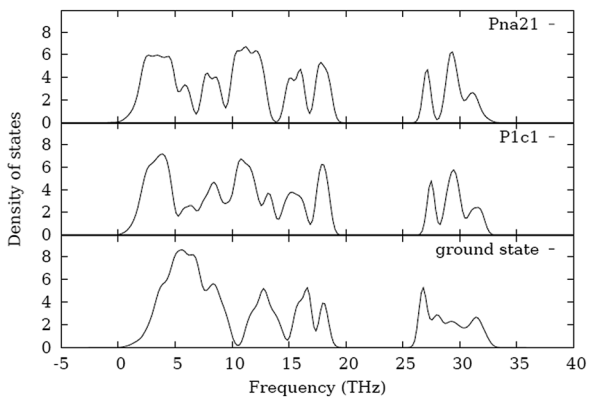

Fig. 9 Density of states of the 3 selected $LiFePO_4$ structures. The bottom one corresponds to the ground state olivine-type structure, the middle one to the second lowest-energy structure from our search results, which is a FeO_4-type structure, and the top one is the third lowest-energy structure, also a FeO_4-type structure from our search results. Both of them are represented using symmetry symbols.

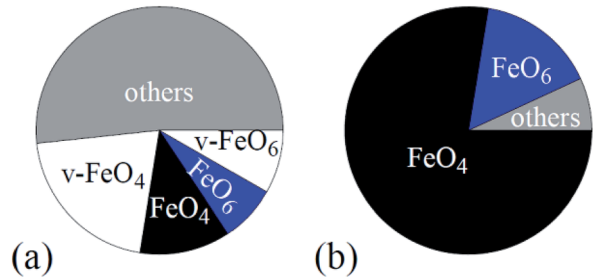

Fig. 10 Pie chart with the percentages of different types of structures (a) within a large energy window up to 0.7 eV/f.u. and (b) within a small energy window under 0.2 eV/f.u.

4. Conclusions

An efficient crystal structure search scheme based on the Fe–P network has been developed for $LiFePO_4$, and a large amount of new low-energy candidate structures have been obtained, which allowed us to build a relatively comprehensive crystal structure database for the $LiFePO_4$ system for further study.

Our method is versatile enough such that it can be applied to complex systems with widely different structural motifs. For instance, it can be easily adapted to enhance structural searches in other systems such as NASICON and LISICON, whose structures have isolated and stable polyhedra similar to PO_4 in $LiFePO_4$. This search scheme represents a highly efficient tool for completing and broadening the representation of various structural databases used for data-mining in material genomics research. The structural dataset and the unveiled rules for identifying low-energy structures can also serve as a prototypical benchmark to test the efficiency and performance of different machine-learning methods.

Compared with the traditional global methods for structure search, such as the genetic algorithm or particle swarm optimization search, the network generation scheme can locate many low-energy structures and provides a more comprehensive view of the low-energy landscape. However, the network scheme requires previous knowledge about the structure to generate candidate configurations, while the global methods for structure search can be performed without previous knowledge.

We explored the low-energy structural landscape of the $LiFePO_4$ system and divided it into two groups according to the Fe–O types of polyhedra. The FeO_4-type structures are energetically comparable to the FeO_6-type, but due to the similar Li and Fe environment in the FeO_4-type structure, Li–Fe switching is

easier in $LiFePO_4$ and therefore, the FeO_4-type structure displays a much richer polymorphism at low energies. However, the existence of the FeO_4-type structures needs to be verified by further experimental work. Furthermore, a set of powerful rules about the relationship between the atom connections and the configuration energy were unveiled. The concept of Fe–P networks in the $LiFePO_4$ system was introduced in our structure generation scheme and was proven useful for describing this system. Studies on the electrochemical properties of $LiFePO_4$ with different Fe–P networks are currently in progress and will be reported in the future.

Appendix

Different Fe–P networks consist of different Fe–P and P–Fe configurations. These configurations are characterized by the coordination number (CN) and angle sequence (AS) of the polyhedra. For a standard FeP_6 octahedron, the CN is 6 and there are 15 P–Fe–P angles. Three of them are 180°, while the other 12 are 90°, resulting in an angle sequence of 180–180–180–90–90–90–90–90–90–90–90–90–90–90–90. Likewise, the CN of a standard FeP_4 tetrahedron is 4 and the AS is 109.5–109.5–109.5–109.5–109.5–109.5. To efficiently perform our bond-angle clustering analysis, we further reduced the AS to two values, which we named as the renormalized angle sequence (RAS). The first value, θ_{max}, is the average of the angles in the AS that are larger than or equal to the average of all angles in the AS (denoted as θ_{avg}). The second one, θ_{min}, is the average of the angles in the AS that are smaller than or equal to θ_{avg}. For example, for the octahedra, the total average (θ_{avg}) of the 15 angles in the AS is 108° and therefore, $\theta_{max} = 180°$ and $\theta_{min} = 90°$, while for a standard tetrahedron, $\theta_{avg} = \theta_{max} = \theta_{min} = 109.5°$. The use of the RAS descriptor for controlling the generation of the Fe–P network reduces sensitivity to distortion of a given Fe–P configuration away from the target, resulting in a more comprehensive exploration of the Fe–P network space.

Cluster analysis according to the RAS of the various configurations corresponding to the ~40 low-energy structures of the MP database indicated that the RAS values are concentrated around several regions within the two-dimensional RAS space. Each region provides a target motif for a given type of Fe-centered or P-centered configuration. For a comprehensive exploration, we also considered some configurations with shapes not found in the MP database. The specific RAS values, angle spread and the corresponding type of configuration are listed in Table 1. For 13 types of averaged configurations obtained from our data analysis. For the FeO_6-type $LiFePO_4$ structures, the Fe–P and P–Fe configurations in the networks have CNs of 4, 5, or 6. For the FeO_4-type structures, the networks only have four-coordinated configurations. The ideal bond lengths and RAS can also vary even for the same Fe–P CN. Thus, a given network is completely characterized by the type of configurations that make it up and the way these configurations are connected. A detailed analysis of the types of Fe–P networks adopted by low-energy $LiFePO_4$ structures will be presented in the future.

Table 1 Parameters for the generation of the Fe–P networks. The tolerance column is for the RAS values. For example, if RAS is set to (120 80) with a tolerance of 3, then 117–123 is the acceptable value of the first RAS term and 77–83 is the acceptable value of the second RAS term. Blanks in the RAS column mean no restriction in this entry. If the Fe–P or P–Fe configurations in a newly generated Fe–P network do not meet the requirements in the table, the network will be discarded

	Configurations	Ideal bond length	RAS		Tolerance
FeO_6	FeP_6	3.4		85	10
	FeP_6	3.4		62	5
	FeP_5	2.95–3.30	130	87	10
	FeP_5	3.3	170	90	5
	FeP_4	2.80–3.27	175	90	10
	FeP_4	2.82–3.30	135	90	10
	PFe_6	3.4	120	77	10
	PFe_5	2.95–3.30	125	80	5
	PFe_4	2.95–3.30		85	5
	PFe_4	2.95–3.30		60	5
FeO_4	FeP_4/PFe_4	2.80–3.30	119	103	10
		3.1	123	83	10
		3.1–3.4		92	5

Whenever multiple networks of a similar type of structure are generated, only one network is retained. The similarity of the network to the target is evaluated using a score function f defined as follows:

$$f = \left\| \vec{x}_0 - \frac{1}{N}\sum_{n=1}^{N} \vec{x}_n \right\|^2 + \sum_{n=1}^{N} (r_n - b_n)^2$$

where for a polyhedron with N vertices, $\vec{x}_0$ is the central atom position; $\vec{x}_n$, r_n and b_n are its n^{th} neighboring atom position, bond length and ideal bond length, respectively. The first term represents the 'off-center' distance between the vertex atom and the geometric center of its neighboring atoms, and the second term represents the deviation of the actual bond length from the ideal target bond length. For a better Fe–P network, we retained the structure with the lowest f score.

A relatively thorough search of the Fe–P network for cell sizes under 1000 Å^3 was performed. The three cell vectors were in the range of about 4.5–11.5 Å. Up to 3 million random cells were explored in each space group out of the total 230. Given a preset range of cell vector length, the code randomly built an empty cell according to the space group restriction. Basically, the are six types of systems: triclinic, monoclinic, orthorhombic, tetragonal, hexagonal and cubic. Each space group belongs to one of these six systems.

For a given space group, after building an empty cell, the cell volume is calculated, and the number of atoms to be introduced into the cell is determined according to the atom density limitation (16–32 atoms per 1000 Å^3). For example, a 330 Å^3 cell should have at least 6 atoms (3 Fe and 3 P) and a maximum of 10 atoms (5 Fe and 5 P).

First, within an empty cell, a random position and its symmetrized positions were arranged with Fe atoms. Then, a P atom was arranged around a randomly selected Fe atom at a specified distance range (2.73–3.70 Å), and the symmetrized positions of the P atom were also arranged with P atoms. Then,

Fe atoms were arranged around P atoms in the same way, and P atoms were subsequently added again around Fe atoms until a Fe–P network with a specified connection was formed. Each time that we added new atoms, the atom distance was checked to avoid a situation where some atoms are too close or there are too many atom connections. For example, if after adding P atoms, the minimal P–P distance was smaller than 3.44 Å, then these P atoms were discarded and rearranged. A specified amount of failures on atom insertion (for example, atoms are too close or there are numerous neighboring atoms) was allowed.

A new network should meet the CN and RAS criteria. Moreover, it should not be a duplicate of a previously saved network. To be efficient, we use the bond distance matrix to remove duplicated networks. For example, given a cutoff distance of 6.5 Å, the Fe–Fe distances were sorted in an ascending order, followed by those of Fe–P and P–P. Subsequently, the bond distance matrix of two networks was compared; if the difference in distances was smaller than the tolerance, then the two networks were considered equal, and the duplicate one was removed (with a worse score).

Each network was embedded with randomly rotated PO_4 tetrahedra in the GA process with a population of 100–150 and 10–15 generations depending on the size of the network. Configurations were relaxed by the classical potential method, with Fe and P atoms being fixed.

Vacancy sites in these $FePO_4$ configurations were examined in a 3D mesh grid along three cell vectors, with each direction divided into segments of 0.5 Å. The Li atom positions in the candidate structures were restricted to those with minimum distances of 2.64 Å to Fe, 2.53 Å to P, 1.69 Å to O, and 2.25 Å to Li. After vacancy sites were identified, Li atoms were randomly added to these positions.

With the network generation scheme, millions of atomic configurations were generated for the $LiFePO_4$ system. To reduce analysis efforts and obtain reliable crystal structures, we only selected atomic configurations with up to 28 atoms and screened them by force field calculations. Firstly, we performed a bond length comparison and energy minimization using the classical potential method to remove duplicate and highly unstable structures. Then, 1200 structures were selected for further examination by DFT calculations using the Vienna *ab initio* Simulation Package (VASP).[16,17] These structures were fully relaxed by the GGA+U method with an effective $U_{\mathrm{eff}} = U - J =$ 4.3 eV for Fe. Moreover, the generalized gradient approximation Perdew–Burke–Ernzerhof[18,19] exchange-correlation functional was applied. An energy cutoff of 520 eV in the plane wave basis and a k-point mesh resolution of $2\pi \times 0.03$ Å^{-1} using the Monkhorst–Pack scheme were applied. In addition, the structures within the energy window of 0.2 eV/f.u. above the ground state phase were selected to perform random Li–Fe switching and only the low-energy structures, within the 0.2 eV/f.u. window, were kept. From all the structures obtained in our search, the three with the lowest energy were selected to perform phonon calculations. The ground state structure (cell vector $a = 4.752$ Å, $b = 6.0874$ Å, $c = 10.4507$ Å) was expanded using a $2 \times 2 \times 1$ supercell (112 atoms), with the expansions performed along the b-axis. The $P1c1$ structure ($a = 8.5620$ Å, $b = 5.1222$ Å, $c = 8.7200$ Å) and the $Pna2_1$ structure ($a = 5.0816$ Å, $b = 6.8656$ Å, $c = 10.2116$ Å) were expanded using a $2 \times 2 \times 2$ supercell (224 atoms). Phonon density of states calculations were performed using the VASP and the Phonopy package.[20] The energy cutoff was 520 eV and the convergence criteria for the total energy was set to 10^{-8} eV.

After DFT relaxation, a robust atomic cluster alignment (ACA) method[21] was used to check the similarity of the final crystal structures based on the geometry and topology of the atomic clusters in the configurations. According to this method, Fe-centered spherical clusters (with 200 atoms) were extracted from the supercells of these configurations and aligned with each other to check for redundant structures. This way, duplicate or similar structures where only the elements are switched were efficiently identified.

In our scheme, we employed the classical EAM[22] potential method for constrained relaxation during the oxygen-rotation process for generating candidate structures and also for removing redundancy in the structure pool before DFT relaxation. The potential we used in this network scheme was obtained in a preliminary AGA[15] search of the $LiFePO_4$ system. The AGA method is based on a combination of the classical potential method and DFT calculations in a genetic algorithm (GA) search for low-energy structure candidates, and the potential

Table 2 EAM potential parameters. Length units are Å and energy units are eV

Embedding function			
	F_0	γ	F_1
Li	−0.0349	1.0000	0.0000
Fe	−0.5442	1.0000	0.0000
P	−0.0009	1.0000	0.0000
O	−12.7433	1.0000	0.0000
Density function			
	α	β	r_0
Li	1.0000	3.1681	1.0000
Fe	1.0000	2.2259	1.0000
P	1.0000	1.6911	1.0000
O	1.0000	7.8455	1.0000
Pair-wise potential			
	ε		σ
Li–Li	5.73×10^{-4}		3.6647
Li–Fe	6.48×10^{-6}		5.3119
Li–P	9.70×10^{-6}		5.1374
Li–O	7.19×10^{-2}		1.8783
Fe–Fe	2.61×10^{-3}		2.8882
Fe–P	3.91×10^{-5}		4.9941
Fe–O	1.60×10^{-5}		3.8279
P–P	3.21×10^{-5}		5.2450
P–O	6.09×10^{-1}		1.3903
O–O	6.54×10^{-6}		5.5413

can be self-corrected by DFT calculations during the iterations of the search process. However, the AGA method is not efficient for this complex system and the classical potential is not accurate enough to locate many low-energy structures, including the ground state one. However, in our network generation scheme, we used this potential to rotate the PO_4 tetrahedra within the $FePO_4$ crystals, with the Fe–P network being fixed, and the classical potential is very powerful when used this way.

The potential is in the EAM[22] form, as shown below. The energy of an atom E_i consists of the embedding part $F(n)$ and the sum of pair interaction parts $V(r_{ij})$. $F(n)$ is a function of the sum of density contribution n from other atoms. $\rho(r)$ denotes each atom density distribution. The pair interactions are expressed by the Lennard-Jones potential. Parameters of this potential are shown in Table 2.

$$E_i = F(n) + \frac{1}{2}\sum_{i\neq j} V(r_{ij})$$

$$F(n) = F_0[1 - \gamma \ln(n)] + F_1 n$$

$$n = \sum_{i\neq j} \rho(r_{ij})$$

$$\rho = \alpha e^{-\beta(r-r_0)}$$

$$V(r) = 4\varepsilon\left[\left(\frac{\sigma}{r}\right)^{12} - \left(\frac{\sigma}{r}\right)^{6}\right]$$

Acknowledgements

Xiaobao Lv acknowledges the support from the USTC and the China Scholarship Council for visiting the Ames Laboratory under File No. 201506340115. Zijing Lin was supported by the National Natural Science Foundation of China (11374272 & 11574284) and the Collaborative Innovation Center of Suzhou Nano Science and Technology. Yongliang Shi acknowledges the support from USTC and the China Scholarship Council for visiting the Iowa State University. Ping Wu and Kai-Ming Ho, from the USTC, were supported by the 111 Project (No. B13027), the USTC Qian-Ren B (1000-Talents Program B) fund, and the Supercomputing Center of the USTC. Work at the Ames Laboratory was supported by the US Department of Energy, Basic Energy Sciences, Division of Materials Science and Engineering, under Contract No. DE-AC02-07CH11358, including a grant of computer time at the National Energy Research Scientific Computing Center (NERSC) in Berkeley, CA. S. Q. Wu, from the Xiamen University, was supported by the National Key Research Program of China (Grant No. 2016YFA0202601), the Natural Science Foundation of the Fujian Province of China (Grant No. 2015J01030) and the Fundamental Research Funds for the Central Universities (Grant No. 20720150034).

References

1 A. K. Padhi, K. S. Nanjundaswamy and J. B. Goodenough, *J. Electrochem. Soc.*, 1997, **144**, 1188–1194.
2 A. Jain, S. P. Ong, G. Hautier, W. Chen, W. D. Richards, S. Dacek, S. Cholia, D. Gunter, D. Skinner, G. Ceder and K. A. Persson, *APL Mater.*, 2013, **1**, 11002.
3 Z. Li, D. Zhang and F. Yang, *J. Mater. Sci.*, 2009, **44**, 2435–2443.
4 C. T. Love, A. Korovina, C. J. Patridge, K. E. Swider-Lyons, M. E. Twigg and D. E. Ramaker, *J. Electrochem. Soc.*, 2013, **160**, A3153–A3161.
5 R. Malik, A. Abdellahi and G. Ceder, *J. Electrochem. Soc.*, 2013, **160**, 3179–3197.
6 J. Wang and X. Sun, *Energy Environ. Sci.*, 2015, **8**, 1110–1138.
7 B. Scrosati and J. Garche, *J. Power Sources*, 2010, **195**, 2419–2430.
8 O. García-Moreno, M. Alvarez-Vega, F. García-Alvarado, J. García-Jaca, J. M. Gallardo-Amores, M. L. Sanjuán and U. Amador, *Chem. Mater.*, 2001, **13**, 1570–1576.
9 X. Zhao, S. Wu, X. Lv, M. C. Nguyen, C.-Z. Wang, Z. Lin, Z.-Z. Zhu and K.-M. Ho, *Sci. Rep.*, 2015, **5**, 15555.
10 Z. Ye, X. Zhao, S. D. Li, S. Q. Wu, P. Wu, M. C. Nguyen, J. H. Guo, J. X. Mi, Z. L. Gong, Z. Z. Zhu, Y. Yang, C. Z. Wang and K. M. Ho, *Electrochim. Acta*, 2016, **212**, 934–940.
11 P. Wu, S. Q. Wu, X. Lv, X. Zhao, Z. Ye, Z. Lin, C. Z. Wang and K. M. Ho, *Phys. Chem. Chem. Phys.*, 2391, **18**, 23916–23922.
12 A. Le Bail, *J. Appl. Crystallogr.*, 2005, **38**, 389–395.
13 D. M. Deaven and K. M. Ho, *Phys. Rev. Lett.*, 1995, **75**, 288.
14 S. Plimpton, *J. Comput. Phys.*, 1995, **117**, 1–19.
15 S. Q. Wu, M. Ji, C. Z. Wang, M. C. Nguyen, X. Zhao, K. Umemoto, R. M. Wentzcovitch and K. M. Ho, *J. Phys.: Condens. Matter*, 2014, **26**, 35402.
16 G. Kresse and J. Furthmüller, *Phys. Rev. B: Condens. Matter Mater. Phys.*, 1996, **54**, 11169–11186.
17 K. Momma and F. Izumi, *J. Appl. Crystallogr.*, 2011, **44**, 1272–1276.
18 J. P. Perdew, K. Burke and M. Ernzerhof, *Phys. Rev. Lett.*, 1996, **78**, 1396.
19 S. L. Dudarev, S. Y. Savrasov, C. J. Humphreys and A. P. Sutton, *Phys. Rev. B: Condens. Matter Mater. Phys.*, 1998, **57**, 1505–1509.
20 A. Togo and I. Tanaka, *Scr. Mater.*, 2015, **108**, 1–5.
21 Y. Sun, F. Zhang, Z. Ye, Y. Zhang, X. Fang, Z. Ding, C.-Z. Wang, M. I. Mendelev, R. T. Ott, M. J. Kramer and K.-M. Ho, *Sci. Rep.*, 2016, **6**, 23734.
22 M. S. Daw and M. I. Baskes, *Phys. Rev. B: Condens. Matter Mater. Phys.*, 1984, **29**, 6443–6453.

